European Journal of Medicinal Chemistry 78 (2014) 140–150

Contents lists available at ScienceDirect

European Journal of Medicinal Chemistry

journal homepage: http://www.elsevier.com/locate/ejmech

Original article

New aminobenzenesulfonamide–thiourea conjugates: Synthesis and carbonic anhydrase inhibition and docking studies

Sumera Zaib [a], Aamer Saeed [b,*], Karin Stolte [c], Ulrich Flörke [c], Mohammad Shahid [d], Jamshed Iqbal [a,e,*]

[a] Centre for Advanced Drug Research, COMSATS Institute of Information Technology, Abbottabad 22060, Pakistan
[b] Department of Chemistry, Quaid-I-Azam University, Islamabad 45320, Pakistan
[c] Department Chemie, Fakultät für Naturwissenschaften, Universität Paderborn, Warburgerstrasse 100, D-33098 Paderborn, Germany
[d] Department of Bioinformatics, Fraunhofer Institute SCAI, Sankt Augustin, Germany
[e] Department of Pharmaceutical Sciences, COMSATS Institute of Information Technology, Abbottabad 22060, Pakistan

ARTICLE INFO

Article history:
Received 25 December 2013
Received in revised form
16 February 2014
Accepted 8 March 2014
Available online 12 March 2014

Keywords:
1-Aroyl/heteroaryl-3-(3-aminosulfonylphenyl)thioureas
3-Aminobenzenesulfonamide
Carbonic anhydrase
Molecular dynamics simulation

ABSTRACT

A variety of 1-substituted-3-(3-aminosulfonylphenyl)thioureas (**3a**–**k**) and two new 1-aroyl-3-(4-aminosulfonylphenyl)thiourea derivatives (**5a** and **5b**) were synthesized by reaction of 3-aminobenzenesulfonamide and 4-aminobenzenesulfonamide respectively with freshly prepared aroyl/heteroaryl isothiocyanates in dry acetonitrile. FTIR, ^{1}H NMR, ^{13}C NMR, GC–MS and elemental analyses data confirmed the assigned structures to the synthesized compounds. Further structure of compound (**3g**) was also confirmed by single crystal XRD analysis. The compounds were investigated as inhibitors of the bovine erythrocyte carbonic anhydrase isoform II (bCA II). The inhibition constants of these compounds against bCA II were in the range 0.011–17.1 μM. Among the evaluated compounds, 1-substituted -3-(3-aminosulfonylphenyl)thiourea derivatives **3h** and **5a** were the most potent inhibitors with IC_{50} of 0.052 and 0.011 μM, respectively. *In silico* docking and molecular dynamics simulation studies were performed against bCA II and human CA II enzymes to rationalize the inhibitory properties of these compounds.

1. Introduction

The zinc metallo-enzyme carbonic anhydrase (CA, EC 4.2.1.1) catalyzes the rapid reversible conversion of carbon dioxide and water into a proton and the bicarbonate ion [1–3]. Carbonic anhydrases are involved in crucial physiological processes connected with transport of CO_2/bicarbonate, homeostasis, electrolyte secretion in a variety of tissues/organs, biosynthetic reactions (such as gluconeogenesis, ureagenesis and lipogenesis), respiration, calcification, tumorigenicity, and bone resorption [1–7]. Deficiency of carbonic anhydrase II is the leading defect in the syndrome of osteoporosis, cerebral calcification and renal tubular acidosis [8]. Inhibition of carbonic anhydrase in the ciliary processes of the eye decreases aqueous humor secretion, most likely by slowing the formation of bicarbonate ions with consequent decrease in sodium and fluid transport. The result is a reduction in intraocular pressure (IOP). Acetazolamide is a well-known example of clinically established carbonic anhydrase inhibitor [9]. Sulfonylureas are amongst the most familiar sulfonamide derivatives possessing potent hypoglycemic activity due to their ability to stimulate the release of insulin from the pancreatic islets. Carbutamide, tolbutamide, chlorpropamide and tolazamide belong to the first generation of sulfonylureas while second generation include glyburide and glipizide [10–12]. Sulfonamides are well known for their diuretic [13], anti-carbonic anhydrase [14] and antimalarial activity [15–17].

Among the broad spectrum of activities exhibited by sulfonamides, their role as inhibitors of the zinc containing metalloenzyme carbonic anhydrase (CA) is presumably most widely studied. Many sulfonamide CA inhibitors have been used as therapeutic agents against various diseases including glaucoma, gastroduodenal ulcers, acid–base disequilibria, and various neurological disorders [18–21].

Thus 4-(3,4-dichloro-phenylureido)thioureido-benzene sulfonamide possessing a thiourea scaffold is an effective *in vitro* inhibitor of carbonic anhydrase; inhibited the *ex vivo* growth of *Plasmodium falciparum* [22]. Several antiplasmodial 7-chloro-4-aminoquinolyl-

* Corresponding author. Centre for Advanced Drug Research, COMSATS Institute of Information Technology, Abbottabad 22060, Pakistan.
E-mail addresses: aamersaeed@yahoo.com (A. Saeed), drjamshed@ciit.net.pk, jamshediqb@gmail.com (J. Iqbal).

http://dx.doi.org/10.1016/j.ejmech.2014.03.023
0223-5234/

derived sulfonamides, ureas, thioureas and amides have been synthesized and tested against chloroquine-resistant (CQR) and chloroquine susceptible (CQS) *P. falciparum* [23].

Previously we have shown sulfanilamide–thiourea hybrids to be effective antimicrobial agents and urease inhibitors [24]. Herein we report synthesis of isomeric 3-aminobenzenesulfonamide appended to thiourea nucleus and their comparison with 4-aminobenzenesulfonamide derivatives. In the present work, we have expanded this new class of inhibitors by synthesizing novel 1-substituted-3-(3-aminosulfonylphenyl)thioureas (**3a**–**k**) and two new 1-aroyl-3-(4-aminosulfonylphenyl)thiourea derivatives (**5a** and **5b**) and determined their inhibition activity against bCA II. Some of the structurally related sulfonamides reported in literature are presented in Fig. 1.

2. Results and discussion

2.1. Chemistry

A variety of aroyl/heteroaryl isothiocyanates (**1a**–**k**) were prepared *in situ* by reaction of corresponding acid chlorides with an equimolar quantity of potassium thiocyanate in dry acetonitrile. Treatment of isothiocyanates with 3-aminobenzenesulfonamide (**2**) in dry acetonitrile in 1:1 M ratio furnished corresponding 1-aroyl/heteroaryl 3-(3-aminosulfonylphenyl)thioureas (**3a**–**k**) in 80–91% yield (Scheme 1). Two new 1-aroyl-3-(4-aminosulfonylphenyl) thioureas **5a** and **5b** were similarly synthesized by reaction of thiophene-2-carbonyl isothiocyanate and coumarin-3-carbonyl isothiocyanate respectively with 4-aminobenzenesulfonamide (**4**) (Scheme 2).

FTIR spectra of the aroyl/heteroaryl substituted thioureas **3a**–**k** and **4a**–**b** were in accordance with those reported for similar compounds [25–27]. In ^{1}H NMR spectra the characteristic singlets for N_1 and N_3 protons were found in a relatively wide range of δ 8.1–9.1 and 10.8–12.1 respectively. The typical differences in the aromatic region of 3-amino and 4-aminobenzenesulfonamides were also noted. Thus, in case of 4-amino compounds (**5a**,**b**) two doublets are observed around 7.81 and 7.90 for aromatic protons, while 3-aminobenzenesulfonamide derivatives (**3a**–**k**), display three to four different signals due to nearly all unequivalent aromatic protons.

Fig. 2 shows the molecular structure of 1-(2-furanyl)-3-(3-aminosulfonylphenyl) thiourea (**3g**) and Table 1 summarizes the main geometric parameters. The furanyl-thiourea moiety is almost planar with a torsion angle O2–C5–C4–C3 of 5.5(3)°. Thiourea torsion angles are O2–C5–N1–C6 1.1(3)°and N2–C6–N1–C5 −1.3(3)°. An intramolecular N2–H…O2 hydrogen bond is connected with that conformation. The furanyl and phenyl rings make a dihedral angle of 22.3(1)°. Other geometric parameters lie in expected ranges. Somewhat related molecular structures are MUWCUD [28] or FAQPOE [29], both with the aminosulfonyl group in para-position and *p*-tolyl or trimethoxyphenyl instead of the furanyl group, respectively. The crystal packing of (**3g**) (Fig. 3) shows intermolecular N1–H…S1 ($-x + 1, -y, -z$) and N3–H31…O4 ($x, -y + 0.5, z-0.5$) interactions that link molecules into pairs of centrosymmetric dimers that are stacked along [001].

2.2. Carbonic anhydrase inhibition

All synthesized compounds were tested for their ability to act as carbonic anhydrase (CA) inhibitors against bovine CA II (bCA-II) isozyme. CA inhibition data for these compounds is given in Table 2. CA inhibitory activities of these compounds were investigated against the standard clinically used inhibitor acetazolamide. The compounds **3a**–**3c** differ only in the relative position of the chloro group on the 3-(3-aminosulfonylphenyl)thioureas ring, have shown IC_{50} values 13.5 ± 1.40, 0.22 ± 0.02 and 5.64 ± 0.09 μM, respectively. Among these chloro group substitution at position 3

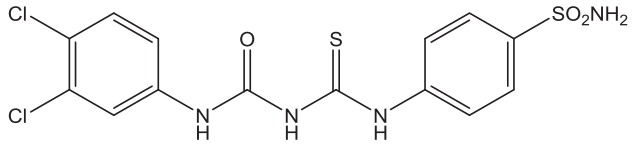

1-(3,4-dichlorophenylcarbamoyl)-3-(4-aminosulfonylphenyl) thiourea

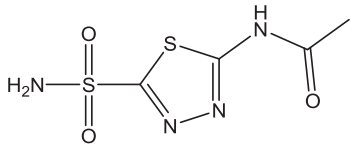

Acetazolamide

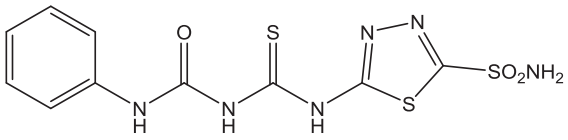

1-(4-1-(3,4-dichlorophenylcarbamoyl)-3-(4-aminosulfonylphenyl) thioureasulphonylaminophenyl)thiourea

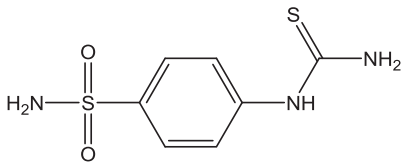

1-(4-aminosulfonylphenyl)thiourea

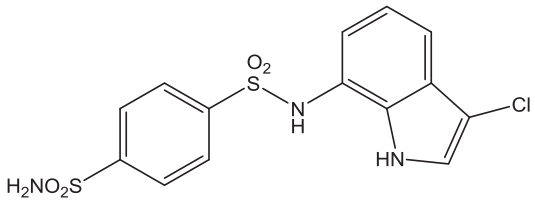

N-(3-chloro-1*H*-indol-7-yl)benzene-1,4-disulfonamide

Fig. 1. Structures of some pharmacologically important related compounds reported in literature.

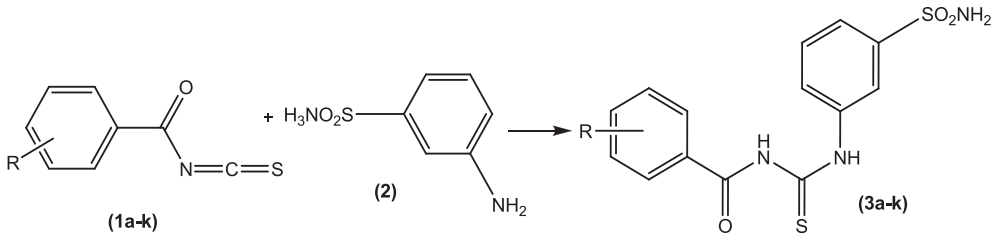

#	R=
3a	2-Cl
3b	3-Cl
3c	4-Cl
3d	2,4-di-Cl
3e	3-NO_2
3f	3,5-NO_2
#	**RPh=**
3g	2-furanyl
3h	2-thiophenyl
3i	1-adamantyl
3j	pivaloyl
3k	coumarin-3-yl

Scheme 1. Synthetic route to 3-aminobenzenesulfonamide–thiourea conjugates (**3a**–**3k**).

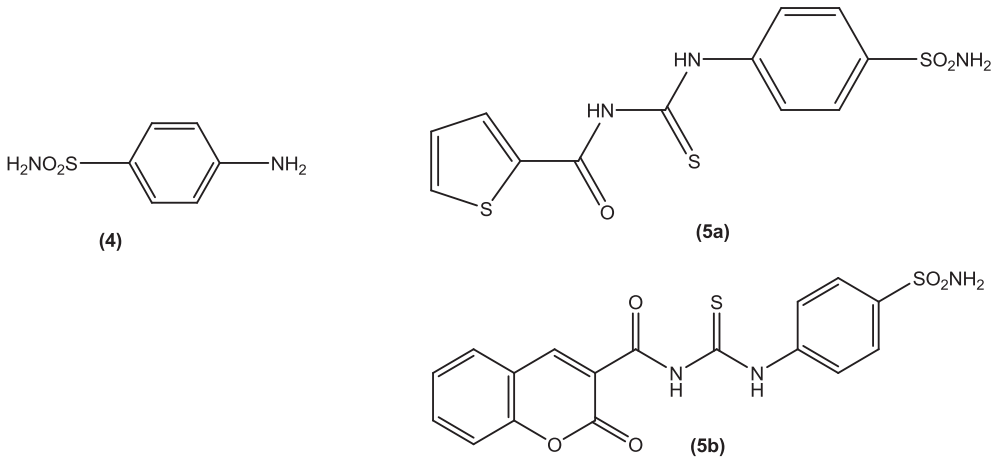

Scheme 2. 4-aminobenzenesulfonamide–thiourea conjugates (**5a, 5b**).

shown maximum IC_{50} value. For compound **3e**, chloro group was replaced by nitro group and IC_{50} value of 0.49 ± 0.01 μM was shown. In case of **3d** and **3f** where di-choloro and di-nitro substituents were present, a significant decrease in inhibition was noticed. As **3d** having di-chloro group attached to the 3-(3-aminosulfonyl-phenyl)thioureas was the least active with IC_{50} value of 17.1 ± 1.81 μM. Compound **3f** has di-nitro group attached to 3-(3-aminosulfonylphenyl)thioureas possessed IC_{50} value of

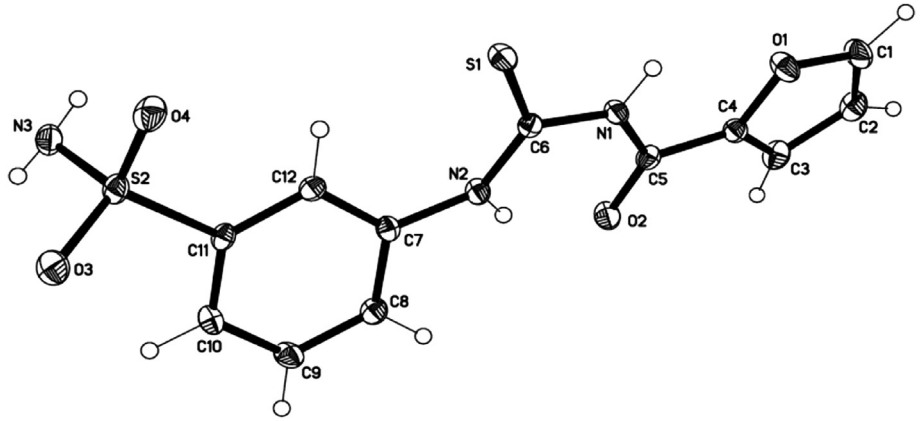

Fig. 2. Molecular structure of 1-(2-furanyl)-3-(3-aminosulfonylphenyl)thiourea (**3g**). Displacement ellipsoids are drawn at the 50% probability level.

Table 1
Selected bond distances (Å) and bond angles (°) for (**3g**).

S1–C6	1.652(2)	N1–C6–N2	113.8(2)
C6–N1	1.407(2)	O2–C5–N1	123.8(2)
C6–N2	1.343(2)	C6–N2–C7	131.9(2)
C5–N1	1.375(2)	N3–S2–C11	108.95(9)
C5–O2	1.231(2)		
S2–C11	1.614(2)	N2–H…S1	2.79
S2–O3	1.436(2)		164.3
S2–O4	1.432(2)	N3–H31…O4	2.19(3)
S2–N3	1.614(2)		166(2)

Table 2
Bovine carbonic anhydrase II inhibition by compounds (**3a**–**3k**, **5a**–**5b**).

Compounds	% Inhibition	$IC_{50} \pm$ SEM (μM)
3a	32.8 ± 0.02[a]	13.5 ± 1.40
3b	78.1 ± 0.01[a]	0.22 ± 0.02
3c	81.2 ± 0.01[b]	5.64 ± 0.09
3d	29.9 ± 0.01[b]	17.1 ± 1.81
3e	70.4 ± 0.02[a]	0.49 ± 0.01
3f	36.4 ± 0.05[a]	14.2 ± 1.22
3g	74.6 ± 0.02[b]	9.76 ± 0.75
3h	73.6 ± 0.01[b]	0.052 ± 0.01
3i	79.6 ± 0.01[b]	5.58 ± 0.69
3j	86.3 ± 0.01[b]	1.28 ± 0.09
3k	39.8 ± 0.02[b]	13.4 ± 1.02
5a	75.9 ± 0.03[a]	0.011 ± 0.001
5b	43.6 ± 0.01[a]	11.3 ± 1.32
Acetazolamide	81.9 ± 0.03[b]	0.96 ± 0.18

[a] 0.1 mM.
[b] 1 mM.

14.2 ± 1.22 μM. In general, compounds containing substituents either chloro or nitro group at meta position were more active. Compounds **3h** and **5a** were the most potent inhibitors having IC_{50} values of 0.052 ± 0.01 and 0.011 ± 0.001 μM, respectively. Compound **3h** having substituent attached to ortho position at 3-(3-aminosulfonylphenyl)thioureas ring possessed IC_{50} value of 0.052 ± 0.01 μM. whereas **5a** having substituent attached to meta position of 3-(4-aminosulfonylphenyl)thioureas ring had IC_{50} value of 0.011 ± 0.001 μM. In general most of compounds in the series have comparable IC_{50} values to that of standard inhibitor (0.96 ± 0.18 μM) used for comparison. However, presence of additional coumarin ring in **3k** and **5b** decreased the activity to 13.4 ± 1.02 and 11.3 ± 1.32 μM, respectively. Substitution of pivaloyl group at 3-(3-aminosulfonylphenyl)thioureas (**3j**) has enhanced the biological activity showing IC_{50} value (1.28 ± 0.09 μM) comparable to the standard inhibitor acetazolamide (0.96 ± 0.18 μM).

2.3. Docking and pose ranking

The results of re-docking experiments showed that the structures were well prepared and the docking program reproduced the natively bound conformations of the co-crystallized bound ligand D7A in both enzyme structures. The NH atom of the sulfamoylbenzamide moiety was in coordination with the Zn^{2+} atom in the re-docking of both enzymes, which was exactly the same in the crystal structure of human carbonic anhydrase II (hCA II). Similarly, the docking results for the compounds **3a**–**3k, 5a**–**5b** were obtained for both enzymes, which showed that there were different conformations (poses) predicted for individual compounds. Table 3 shows the docking scores obtained with FlexX docking and the rank number of best pose obtained with NNScore algorithm for the compounds screened against both bCA II and hCA II enzymes. Docking scores of the compounds were not used to filter the poses of compounds docked into both enzymes; however, filtering the poses for the compounds by NNScore showed there could be other conformations that might interact favorably with the enzymes. The favorable binding modes for most of the compounds revealed the interaction of the deprotonated nitrogen of the sulfonamide moiety of the compounds. It was, therefore, observed that selected pose was not always the first ranking pose based on docking scores.

2.3.1. Binding mode analysis

A common binding mode was observed for the compounds docked to both enzymes. The selected docked conformations form the same interactions with the metal atom and the important residues in the active catalytic site of bCA II. The deprotonated N of sulfonamide moiety coordinates well with the Zn^{2+} and the aromatic ring is involved in hydrophobic and aromatic interactions with His63, His93, His95 and Thr198. The oxygen atom of the sulfonamide part is also involved in hydrogen bond interactions with Thr197 and Thr198. This is similar to the interaction of co-crystalized ligand D7A with Thr199 in hCA II enzyme. Another frequent interaction observed in most of the

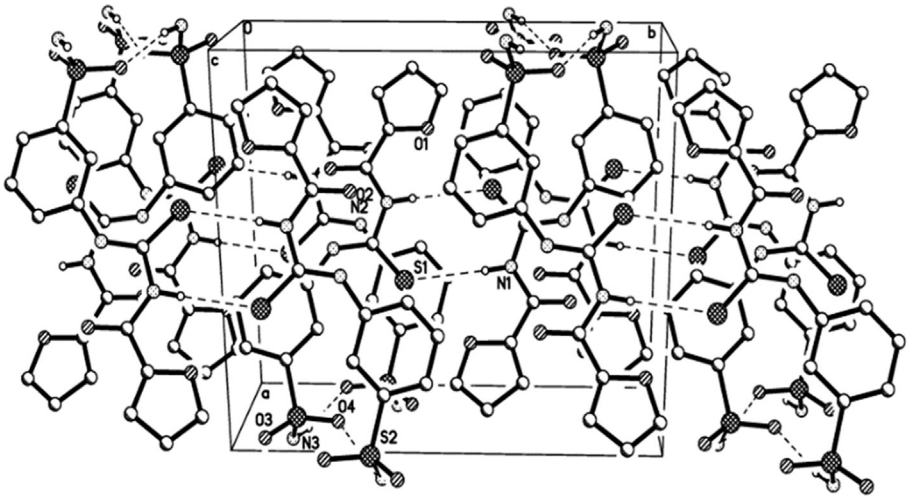

Fig. 3. Crystal packing of 1-(2-furanyl)-3-(3-aminosulfonylphenyl)thiourea (**3g**) viewed along c-axis showing hydrogen bonding pattern as dotted lines. H-atoms not involved are omitted.

Table 3
Docking scores and best pose ranks for the compounds (**3a**–**3k**, **5a**–**5b**) screened against bCA II and hCA II.

Compounds	Docking scores (kcal/mol)		Pose ranks in top 10	
	bCA II	hCA II	bCA II	hCA II
3a	−24.82	−18.57	8	7
3b	−24.25	−21.03	8	9
3c	−21.12	−23.57	4	1
3d	−24.18	−9.75	2	6
3e	−23.40	−30.56	7	1
3f	−20.53	−22.02	3	7
3h	−24.45	−18.01	10	9
3i	−18.73	−17.31	8	3
3j	−18.67	−21.55	1	1
3k	−25.30	−24.09	9	10
5a	−24.21	−27.74	8	5
5b	−22.82	−20.18	8	4

docked compounds is the hydrogen bonding interaction of the two nitrogen atoms in the thiourea moiety of the compounds which form hydrogen bonds with Gln91 residue as shown in Fig. 4. The preferred binding modes selected by external scoring function reveal that most of the compounds interact in a very similar way in the catalytic site of the enzyme. The correct coordination with the Zn^{2+}, aromatic interaction with His93 and hydrogen bond interaction with Thr198 is also similar to the interactions made by the respective native bound ligand of the hCA II enzyme as shown in Fig. 5. Hydrophobic interactions are also observed with Val90 and Phe129 situated at the entrance of the catalytic site of the enzyme. It can be concluded that the predicted binding poses that are filtered by the external scoring function are interacting in a similar way and these binding modes are favored according to the nature of the active site pockets of both enzymes as indicated in Fig. 6.

2.3.2. Molecular dynamics simulations

Individual molecular dynamics simulations were conducted for all the selected poses of the compounds against both bCA II and hCA II enzymes. Each protein–ligand complex was parameterized for the high-ranking pose that was filtered and selected by NNScore. The pre-equilibration steps (temperature and density) and final equilibration results showed that the complexes were equilibrated as shown in Fig. 7, and the enzyme–ligand complexes can be further simulated to obtain enough samples for computing free energy of binding values as well as determine the stability of the binding modes. Equilibration plots for all enzyme–ligand complexes of bCA II and hCA II are shown in Fig. 8.

The distance plots shown in Fig. 9 represent the interatomic distances between the N atom of the sulfonamide part of the molecules and the Zn^{2+} atom during the time period of MD simulation. The distances show that the initial bound conformation of the compounds in which the N atom coordinates with the Zn^{2+} atom remains the same during the simulation, however, for two compounds **3c** and **3f**, their distances increases from the Zn^{2+} atom in the beginning of MD simulation in the case of bCA II complex. However, the conformation changes back again after 2 ns simulation. Similarly the distance between these atoms for compound **3f** inside hCA II enzyme also changes after 4 ns of MD simulation. These findings suggests that for some compounds, the conformational changes should be observed for a longer simulation time to find the comparatively favorable conformation that persists longer during the simulation time.

2.3.3. Free energy of binding

The free energy of binding values estimated with MM-PBSA method for all compounds against both bCA II and hCA II enzymes are given in Table 4. The estimated ΔG values showed that the most of the compounds interact with a good binding energy range inside the active catalytic sites of both enzymes. Furthermore, the free energy of binding values also correlate positively with the experimentally derived ΔG values from IC_{50} (μM) values. The observed correlations of estimated ΔG and experimental ΔG is 0.52 for bCA II and 0.66 for hCA II, respectively. These results show that MM-PBSA based method to systematically evaluate free energy of binding for a series of compounds can provide a good estimate of the relative binding free energies.

3. Conclusion

Several novel 1-aroyl-3-(3-aminosulfonylphenyl)thiourea derivatives (**3a**–**k**) and two new 1-aroyl-3-(4-aminosulfonylphenyl) thioureas (**5a** and **5b**) were synthesized which differ from most of

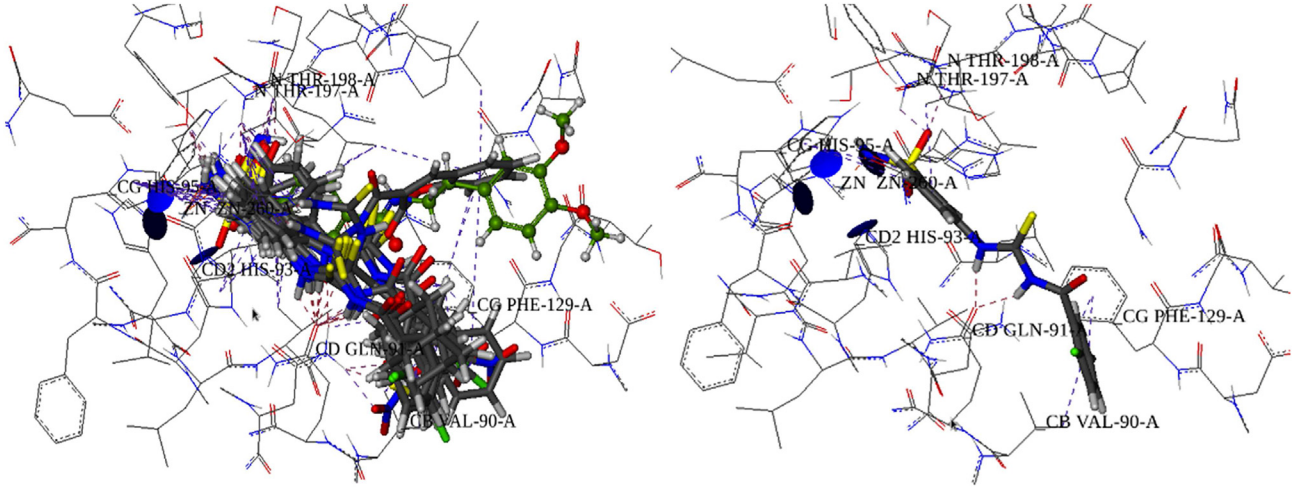

Fig. 4. Binding modes and interactions of the compounds inside the active site of bCA II. Compounds are shown in CPK model and the imported co-crystal ligand D7A is shown in ball & sphere model in green color. Blue circles represent the coordination geometry around the Zn^{2+} atom. Left: Preferred binding modes for the compounds **3a**–**3k** docked into the active site of bCA II. Right: Predicted conformation of compound **3a** inside the active site of bCA II. (For interpretation of the references to colour in this figure legend, the reader is referred to the web version of this article.)

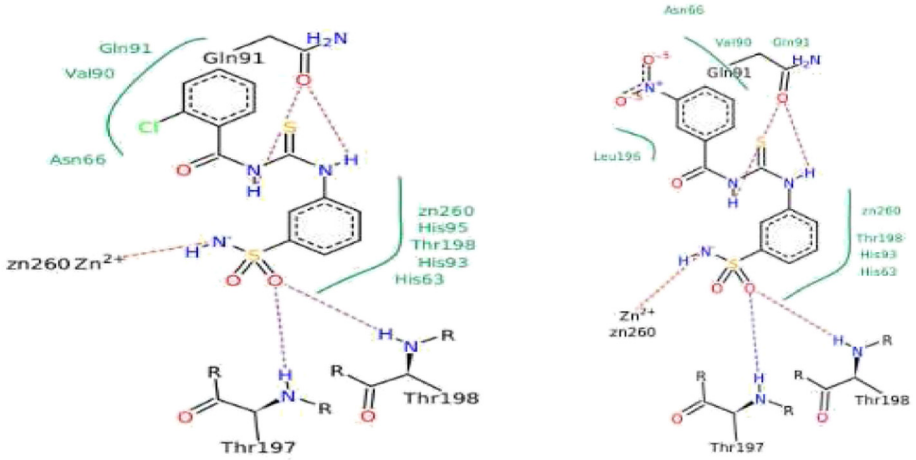

Fig. 5. Interaction diagrams of the selected docked conformations for compounds **3a** and **3e** inside the active site of bCA II enzyme. Hydrogen bond interactions are shown with dotted lines in red and hydrophobic interactions are drawn with green lines. (Left): Interaction diagram of compound **3a**. (Right): Interaction diagram of compound **3e**. (For interpretation of the references to colour in this figure legend, the reader is referred to the web version of this article.)

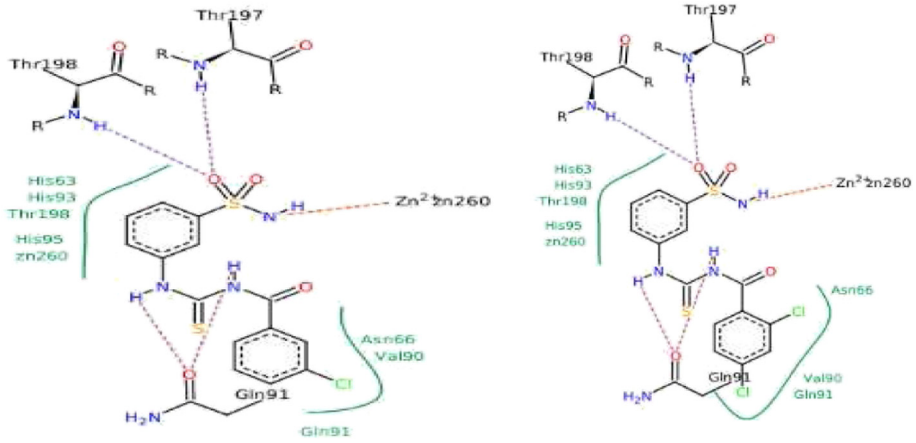

Fig. 6. Interaction diagrams of the selected docked conformations for compounds **3b** and **3d** inside the active site of bCA II enzyme. Hydrogen bond interactions are shown with dotted lines in red and hydrophobic interactions are drawn with green lines. (Left): Interaction diagram of compound **3b**. (Right): Interaction diagram of compound **3d**. (For interpretation of the references to colour in this figure legend, the reader is referred to the web version of this article.)

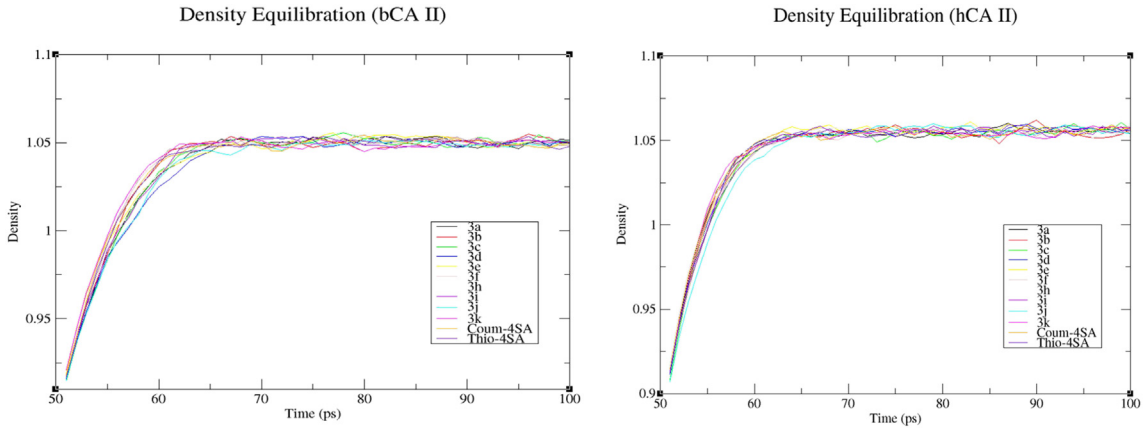

Fig. 7. Density plots showing density equilibrations for all individual enzyme–ligand complexes. (Left) Density plots for all compounds during pre-equilibration step for bCA II complexes. (Right): Density plots for all compounds during pre-equilibration step for hCA II complexes.

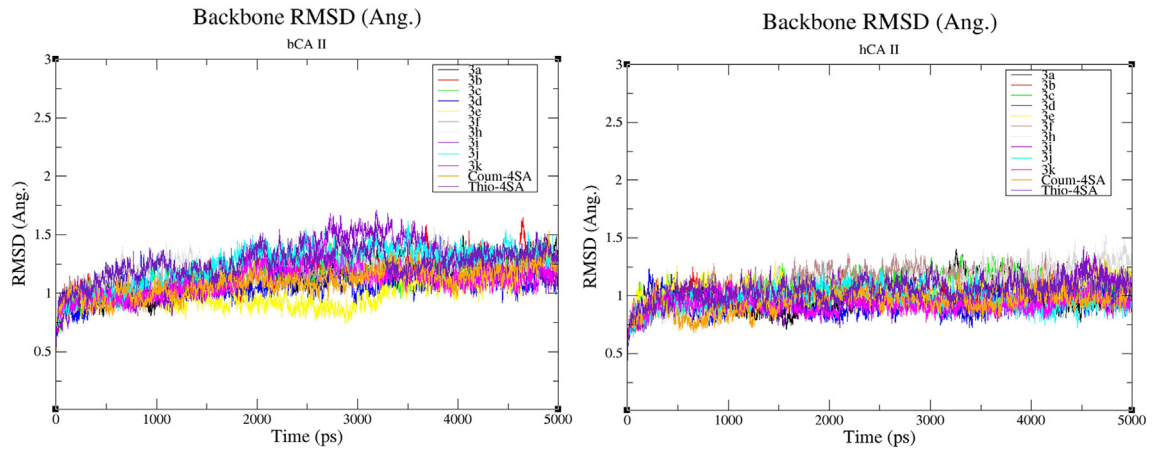

Fig. 8. Equilibration plots for all enzyme–ligand complexes of bCA II and hCA II. RMSD deviations in backbone atoms show that the complexes start to equilibrate after 2 ns of MD simulation. (Left): Backbone RMSD plots of compounds simulated with bCA II. (Right): Backbone RMSD plots of compounds simulated with hCA II.

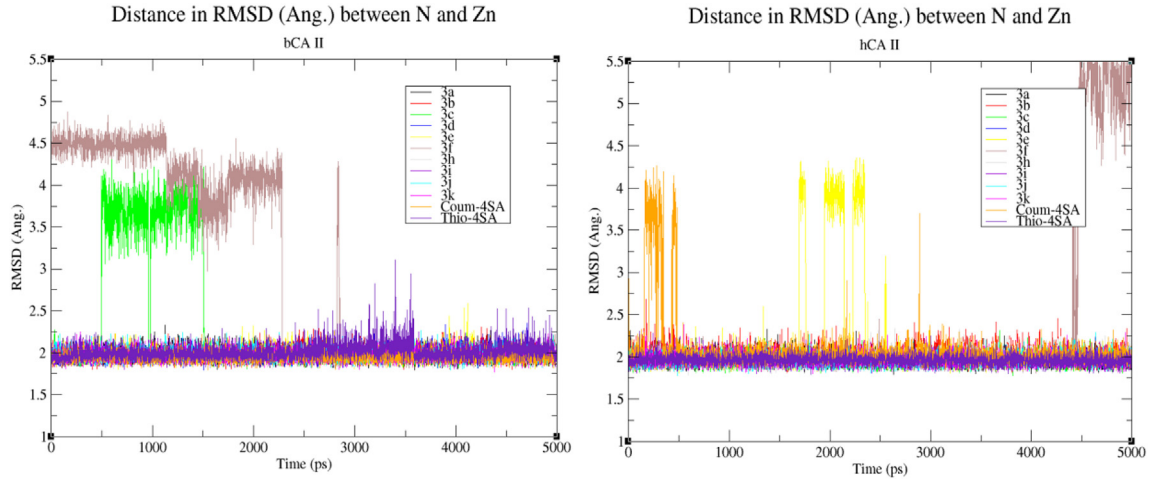

Fig. 9. Plots showing distance measurements between ligand's N atom of sulfonamide group and Zn^{2+} atom for all enzyme–ligand complexes of bCA II and hCA II. (Left): Distance plots for compounds simulated with bCA II. (Right): Distance plots of compounds simulated with hCA II.

the known sulfonyl thiourea derivatives in having the anilino nitrogen of sulfanilamide being incorporated into the thiourea nucleus leaving the sulfonamide amino group intact. Some of the compounds investigated exhibited excellent CA inhibitory activity in the lower micromolar range. Compounds **3h** and **5a** were potent CA II inhibitors with IC_{50} values 0.052 ± 0.01 and 0.011 ± 0.001 μM, respectively. Further, these finding suggest that novel thioureas derivatives may be used for further investigation on a wide range of CA isozymes which are important drug targets in drug development.

Table 4
Experimental and estimated free energy (Δ*G* values) calculated for all compounds simulated with bCA II and hCA II enzymes.

Compounds	Experimental Δ*G* (kcal/mol)	Estimated Δ*G* (kcal/mol) MM-PBSA	Estimated Δ*G* (kcal/mol) MM-GBSA	Estimated Δ*G* (kcal/mol) MM-PBSA	Estimated Δ*G* (kcal/mol) MM-GBSA
	bCA II	bCA II	bCA II	hCA II	hCA II
3a	−6.58	−8.64	−50.72	−9.52	−55.09
3b	−8.99	−15.5	−56.11	−17.25	−71.32
3c	−7.09	−14.34	−56.99	−13	−62.28
3d	−6.44	−9.93	−52.79	−2.38	−11.45
3e	−8.52	−10.33	−51.82	−14.77	−62.61
3f	−6.55	−10.17	−58.06	−4.23	−47.21
3h	−9.86	−13.85	−54.71	−10.48	−49.42
3i	−7.09	−13.23	−55.7	−10.98	−64.97
3j	−7.09	−15.27	−48.81	−12.51	−60.64
3k	−7.96	−8.51	−52.63	−11.63	−55.41
5a	−6.68	−15.81	−62.95	−12.94	−47.29
5b	−10.80	−18.96	−62.25	−18.26	−65.94
Correlation	–	0.52	0.26	0.66	0.44

4. Experimental

4.1. Instrumentation

Melting points were recorded using a digital Gallenkamp (SANYO) model MPD.BM 3.5 apparatus and are uncorrected. ^{1}H NMR spectra were determined as $CDCl_3$ solutions at 300 MHz using a Bruker AM-300 spectrophotometer using TMS as an internal reference and ^{13}C NMR spectra were determined at 75 MHz in DMSO-d_6. FTIR spectra were recorded on an FTS 3000 MX spectrophotometer. Mass Spectra (EI, 70 eV) on a MAT 312 instrument, and elemental analyses were conducted using a LECO-183 CHNS analyzer.

4.2. Synthesis of 1-aroyl/heteroaryl-3-(3-aminosulfonylphenyl) thioureas (3a–3m) and 1-heteroaryl-3-(4-aminosulfonylphenyl) thioureas (**5a, 5b**)

A solution of suitably substituted aroyl//heteroaryl/acyl chloride (10 mmol) in dry acetonitrile (50 mL) was added dropwise to a suspension of potassium thiocyanate (10 mmol) in acetonitrile (30 mL) and the reaction mixture was refluxed for 30 min to afford isothiocyanates (**1a**–**k**). After cooling to room temperature, a solution of 3-aminobenzenesulfonamide (**2**) (10 mmol) or 4-aminobenzenesulfonamide (**4**) (10 mmol) (in case of **5a** and **5b**) in dry acetonitrile (10 mL) was added and the resulting mixture refluxed for 1–3 h. The reaction mixture was then poured into cold water and the precipitated thioureas (**3a**–**3m** and **5a**, **5b**) were recrystallized using aqueous ethanol.

4.2.1. 1-(2-Chorobenzoyl)-3-(3-aminosulfonylphenyl)thiourea (**3a**)

Yield: (87%); m.p. 341 °C; IR (Pure) υ cm^{-1}: 3293 (NH), 1665 (C=O), 1591 (C=C), 1542 (thioamide I), 1332 (C–S), 1245 (thioamide II), 1158, 1091 (thioamide III), 750 (thioamide IV) ^{1}H NMR (δ ppm, J Hz): 12.81 (s, 1H, NH), 11.7 (s, 1H, NH), 7.42 (SO_2NH_2), 7.9 (d, 2H, Ar, J = 6.1), 7.15 (d, 2H, Ar, J = 6.5), 7.62 (d, 2H, Ar, J = 6.3), 6.5 (d, 2H, Ar, J = 5.9) ^{13}C NMR (δ ppm) 180 (C=S), 173 (C=O), 157 (C–Cl), 139 (C–N), 136 (C–CO), 133 (Ar), 131 (Ar), 129 (Ar), 128 (Ar), 127 (Ar), 126 (Ar), 124 (Ar), 122 (Ar), 121 (Ar). Anal. Calcd. For $C_{14}H_{12}ClN_3O_3S_2$: C, 45.46; H, 3.27; N, 11.36; S, 17.34%; Found C, 45.39; H, 3.23; N, 11.27; S, 17.36%; EIMS m/z (%): 369 [M$^+$], 171 (56), 119 (100).

4.2.2. 1-(3-Chorobenzoyl)-3-(3-aminosulfonylphenyl)thiourea (**3b**)

Yield: (87%); m.p. 221–222 °C IR (Pure) υ cm^{-1}: 3293 (NH), 1665 (C=O), 1591 (C=C), 1542 (thioamide I), 1332 (C–S), 1245 (thioamide II), 1158, 1091 (thioamide III), 750 (thioamide IV) ^{1}H NMR (δ ppm, J Hz): 12.81 (s, 1H, NH), 11.7 (s, 1H, NH), 7.9 (d, 2H, Ar, J = 6.1), 7.15 (d, 2H, Ar, J = 6.5), 7.62 (d, 2H, Ar, J = 6.3), 6.5 (d, 2H, Ar, J = 5.9) ^{13}C NMR (δ ppm) 180 (C=S), 173 (C=O), 157 (C–F), 139 (C–N), 136 (C–CO), 133 (Ar), 131 (Ar), 129 (Ar), 128 (Ar), 127 (Ar), 126 (Ar), 124 (Ar), 122 (Ar), 121 (Ar). Anal. Calcd. For $C_{14}H_{12}ClN_3O_3S_2$: C, 45.46; H, 3.27; N, 11.36; S, 17.34%; Found C, 45.42; H, 3.36; N, 11.29; S, 17.38%; EIMS m/z (%): 369 [M$^+$], 371, 171 (56), 119 (100).

4.2.3. 1-(4-Chorobenzoyl)-3-(3-aminosulfonylphenyl)thiourea (**3c**)

Yield: (71%); m.p 221 °C; IR (Pure) υ: 3287 (NH), 1665 (C=O), 1590 (C=C), 1525 (thioamide I), 1325 (C–S), 1254 (thioamide II), 1158, 1011 (thioamide III), 754 (thioamide IV) cm^{-1}; ^{1}H NMR (δ ppm, J Hz): 12.8 (s, 1H, NH), 11.3 (s, 1H, NH), 7.9 (d, 2H, Ar), 7.11 (d, 2H, Ar, J = 5.5), 7.42 (SO_2NH_2), 7.62 (d, 2H, Ar, J = 5.9), 6.45 (d, 2H, Ar, J = 4.5); ^{13}C NMR (δ ppm) (75 MHz) δ: 179 (C=S), 171 (C=O), 139 (C–S), 138.1 (C–Cl), 136 (C–CO), 133 (Ar), 131 (Ar), 129 (Ar), 128 (Ar), 127 (Ar), 126 (Ar), 124 (Ar), 122 (Ar), 121 (Ar); Anal. Calcd. For $C_{14}H_{12}ClN_3O_3S_2$: C, 45.46; H, 3.27; Cl, 9.59; N, 11.36; S, 17.34%; Found C, 45.51; H, 3.32; Cl, 9.53; N, 11.30; S, 17.29%; EIMS m/z (%):369 [M$^+$], 371, 171 (56), 119 (100), 91 (65).

4.2.4. 1-(3,4-Dichlorobenzoyl)-3-(3-aminosulfonylphenyl) thiourea (**3d**)

Yield: (83%); m.p 180 °C; IR (Pure) υ: 3245 (NH), 1660 (C=O), 1590 (C=S), 1531 (thioamide I), 1330 (C–S), 1234 (thioamide II), 1151, 1097 (thioamide III), 747 (thioamide IV) cm^{-1}; ^{1}H NMR (δ ppm, J Hz): 12.91 (s, 1H, NH), 11.93 (s, 1H, NH), 7.85 (m, 1H, Ar), 7.51 (m, 1H, Ar), 7.41 (m, 3H, Ar, SO_2NH_2), 7.62 (d, 2H, Ar, J = 6.3), 6.5 (d, 2H, Ar, J = 5.9); ^{13}C NMR (δ ppm): 180 (C=S), 173 (C=O), 144.1, 139 (C–N), 136 (C–CO), 133 (Ar), 131 (Ar), 129 (Ar), 128 (Ar), 127 (Ar), 126 (Ar), 124 (Ar), 109.4, 108.7. Anal. Calcd. For $C_{14}H_{11}Cl_2N_3O_3S_2$: C, 41.59; H, 2.74; N, 10.39; S, 15.86%; Found: C, 41.62; H, 2.71; N, 10.43, S, 15.81%; GC–MS m/z: 402.96, 404.96 (M$^{\cdot+}$).

4.2.5. 1-(3-Nitrobenzoyl)-3-(3-aminosulfonylphenyl)thiourea (**3e**)

Yield: (88%); m.p 260 °C; IR (Pure) υ: 3350 (NH), 1670 (C=O), 1594 (C=C), 1462 (thioamide I), 1326 (C–S), 1257 (thioamide II), 1155, 1072 (thioamide III), 750 (thioamide IV) cm^{-1}; ^{1}H NMR (δ ppm, J Hz): 12.2 (s, 1H, NH), 11 (s, 1H, NH), 7.69 (d, 2H, Ar, J = 6.2), 7.42 (m, 3H, Ar, SO_2NH_2), 6.54 (d, 2H, Ar, J = 5.2), 6.42 (d, 2H, Ar, J = 4.9), 6.2 (d, 2H, Ar, J = 5.9); ^{13}C NMR (δ ppm) (75 MHz) δ: 179 (C=S), 171 (C=O), 150.8 (C–NO_2), 139 (C–S), 136 (C–CO), 133 (Ar), 132 (Ar), 131 (Ar), 129 (Ar), 128 (Ar), 127 (Ar), 126 (Ar), 124 (Ar), 122 (Ar); Anal. Calcd. For $C_{14}H_{12}N_4O_5S_2$: C, 44.20; H, 3.18; N, 14.73; S, 16.86%; Found C, 44.20; H, 3.18; N, 14.73; S, 16.86%; EIMS m/z (%): 380 [M$^+$], 214 (1), 171 (56), 119 (100), 91 (65).

4.2.6. 1-(3,5-Dinitrobenzoyl)-3-(3-aminosulfonylphenyl)thiourea (**3f**)

Yield: (88%); m.p 194–196 °C; IR (Pure) υ: 3350 (NH), 1670 (C=O), 1594 (C=C), 1462 (thioamide I), 1326 (C–S), 1257 (thioamide II), 1155, 1072 (thioamide III), 750 (thioamide IV) cm^{-1}; ^{1}H NMR (δ ppm, J Hz): 12.2 (s, 1H, NH), 11 (s, 1H, NH), 7.69 (d, 2H, Ar, J = 6.2), 7.44 (SO_2NH_2), 6.54 (d, 2H, Ar, J = 5.2), 6.42 (d, 2H, Ar, J = 4.9), 6.2 (d, 2H, Ar, J = 5.9); ^{13}C NMR (δ ppm) (75 MHz) δ: 179 (C=S), 171 (C=O), 150.8 (C–NO_2), 139 (C–S), 136 (C–CO), 133 (Ar), 132 (Ar), 131 (Ar), 129 (Ar), 128 (Ar), 126 (Ar), 124 (Ar), 122 (Ar); Anal. Calcd. For $C_{14}H_{12}N_4O_5S_2$: C, 44.20; H, 3.18; N, 14.73; S, 16.86%; Found C, 44.20; H, 3.18; N, 14.73; S, 16.86%; EIMS m/z (%): 380 [M$^+$], 214 (1), 171 (56), 119 (100), 91 (65).

4.2.7. 1-(2-Furanylcarbonyl)-3-(3-aminosulfonylphenyl)thiourea (**3g**)

Yield: (78%); m.p 200–203 °C; IR (Pure) υ: 3245 (NH), 1660 (C=O), 1590 (C=S), 1531 (thioamide I), 1330 (C–S), 1234 (thioamide II), 1151, 1097 (thioamide III), 747 (thioamide IV) cm^{-1}; ^{1}H NMR (δ ppm, J Hz): 12.78 (s, 1H, NH), 11.6 (s, 1H, NH), 7.51 (d, 1H, furanyl, J = 5.1), 7.42 (SO_2NH_2), 6.7 (d, 1H, furanyl, J = 6.5), 6.67 (d, 1H, furanyl, J = 6.5), 7.62 (d, 2H, Ar, J = 6.3), 6.5 (d, 2H, Ar, J = 5.9); ^{13}C NMR (δ ppm): 180 (C=S), 173 (C=O), 144.1 (furanyl), 139 (C–N), 136 (C–CO), 133 (Ar), 131 (Ar), 129 (Ar), 128 (Ar), 127 (Ar), 126 (Ar), 124 (Ar), 109.4 (furanyl), 108.7 (furanyl); Anal. Calcd. For $C_{11}H_{11}N_3O_3S_2$: C, 44.43; H, 3.73; N, 14.13; S, 21.57%; Found: C, 44.39; H, 3.81; N, 14.07; S, 21.64%; GC–MS m/z: 297.02 (M$^{\cdot+}$, 100).

4.2.8. 1-(2-Thienylcarbonyl)-3-(3-aminosulfonylphenyl)thiourea (**3h**)

Yield: (78%); m.p 102 °C; IR (Pure) υ: 3245 (NH), 1660 (C=O), 1590 (C=S), 1531 (thioamide I), 1330 (C–S), 1234 (thioamide II), 1151, 1097 (thioamide III), 747 (thioamide IV) cm^{-1}; ^{1}H NMR (δ ppm, J Hz): 11.8 (s, 1H, NH), 9.6 (s, 1H, NH), 7.51 (d, 1H, thiophenyl, J = 5.3), 7.42 (SO_2NH_2), 6.73 (d, 1H, thiophenyl, J = 6.51), 6.67 (d, 1H, thiophenyl, J = 6.5), 7.62 (d, 2H, Ar, J = 6.3), 6.51 (d, 2H, Ar, J = 5.9);

^{13}C NMR (δ ppm): 180 (C═S), 173 (C═O), 144.1 (thiophenyl), 139 (C–N), 136 (C–CO), 133 (Ar), 131 (Ar), 129 (Ar), 128 (Ar), 127 (Ar), 126 (Ar), 124 (Ar), 107.9 (thiophenyl), 108.2 (thiophenyl); Anal. Calcd. For $C_{12}H_{11}N_3O_3S_3$: C, 42.22; H, 3.25; N, 12.31; S, 28.17%; Found: C, 42.22; H, 3.25; N, 12.31; S, 28.17%; GC–MS *m/z*: 342 ($M^{\cdot+}$, 13).

4.2.9. 1-(1-Adamantylcarbonyl)-3-(3-aminosulfonylphenyl) thiourea (**3i**)

Yield: (78%); m.p 197–198 °C; IR (Pure) υ: 3245 (NH), 1660 (C═O), 1590 (C═S), 1531 (thioamide I), 1330 (C–S), 1234 (thioamide II), 1151, 1097 (thioamide III), 747 (thioamide IV) cm^{-1}; ^{1}H NMR (δ ppm, *J* Hz): 12.71 (br s, 1H, NH, D_2O exchangeable); 7.63 (br s, 1H, NH, D_2O exchangeable); 7.23–7.33 (m, 2H, Ar); 7.38–7.43 (m, 2H, Ar), 7.39 (SO_2NH_2), 8.40–8.48 (m, 1H, Ar); 2.08 (s, 3H, adamantane-CH), 1.69 (s, 6H, adamantane-CH_2), 1.58 (q, 6H, adamantane-CH_2, J = 8.6 Hz); ^{13}C NMR (75 MHz, $CDCl_3$): 179.6 (C═S); 170.12 (C═O); 143.05 (C-9); 41.51, 39.25, 38.69, 38.49, 36.44, 36.14, 28.05, 27.86, 27.78, (adamantane-C); Anal. Calcd for $C_{18}H_{23}N_3O_3S_2$: C, 54.94; H, 5.89; N, 10.68; S, 16.29%; Found: C, 54.94; H, 5.89; N, 10.68; S, 16.29%. GC–MS *m/z*: 393.2 ($M^{\cdot+}$, 54).

4.2.10. N-(3-Sulfamoylphenylcarbamothioyl)pivalamide (**3j**)

Yield: (83%): m.p 109 °C; IR (Pure) υ: 3245 (NH), 1660 (C═O), 1590 (C═S), 1531 (thioamide I), 1330 (C–S), 1234 (thioamide II), 1151, 1097 (thioamide III), 747 (thioamide IV) cm^{-1}; ^{1}H NMR (δ ppm, *J* Hz): 12.91 (s, 1H, NH), 11.93 (s, 1H, NH), 8.13 (1H, brs), 7.59 (1H, t J = 7.8 Hz), 7.68 (1H, d, J = 7.5 Hz), 7.81 (1H, d, J = 7.5 Hz), 8.13 (1H, brs) 7.42 (SO_2NH_2), 1.26 (s, 3H, ^{t}Bu); ^{13}C NMR (δ ppm): 185.5 (C═S), 184.9 (C═O), 126.79, 126.81, 126.84, 133.0, 134.6, 143.6, 149.6, 44.67 (merged with DMSO-d_6 signal). 31.5; Anal. Calcd. For $C_{12}H_{17}N_3O_3S_2$: C, 45.70; H, 5.43; N, 13.32; S, 20.33%; Found: C, 45.67; H, 5.45; N, 13.29; S, 20.28%; GC–MS *m/z*: 315.0 ($M^{\cdot+}$).

4.2.11. 1-(-Oxo-2H-chromene-3-carbonyl)-3-(3-aminosulfonylphenyl)thiourea (**3k**)

Yield: (68%); m.p. 192–196 °C; IR (pure, cm^{-1}): 3250 (NH), 1725, 1685 (2C═O), 1558 (C═C), 1253 (C═S); ^{1}H NMR (300 MHz): δ12.20 (s, 1H, NH), 11.84 (s, 1H, NH), 10.75 (s, 1H, C–H, *H*-4), 7.70 (d, 1H, J = 7.5 Hz, *H*-8), 7.43–7.37 (m, 4H, *H*-7, *H*-6, SO_2NH_2), 6.89 (d, 1H, J = 7.8 Hz, *H*-5); ^{13}C NMR (75.5 MHz, DMSO): δ 187.0, 168.3, 159.5, 150.2, 138.6, 128.4, 126.6, Anal. Calcd. For $C_{17}H_{13}N_3O_5S_2$: C, 50.61; H, 3.25; N, 10.42; S, 15.89%; Found: C, 50.57; H, 3.21; N, 10.40; S, 15.92%; GC–MS *m/z*: 403.1 ($M^{\cdot+}$).

4.2.12. 1-(-Oxo-2H-chromene-3-carbonyl)-3-(4-aminosulfonylphenyl)thiourea (**5a**)

Yield: (68%); m.p. 206 °C; IR (pure, cm^{-1}): 3250 (NH), 1725, 1685 (2C═O), 1558 (C═C), 1253 (C═S); ^{1}H NMR (300 MHz): δ12.20 (s, 1H, NH), 11.84 (s, 1H, NH), 10.75 (s, 1H, C–H, *H*-4), 7.70 (d, 1H, J = 7.5 Hz, *H*-8), 7.81 (d, 2H, Ar, J = 6.5), 7.89 (d, 2H, Ar, J = 6.1), 6.89 (d, 1H, J = 7.8 Hz, *H*-5); ^{13}C NMR (75.5 MHz, DMSO): δ 187.0, 168.3, 159.5, 150.2, 142.6, 129.4, 126.6, 122.0, 126.6, 119.2, 118.20, 115.20 Anal. Calcd. For $C_{17}H_{13}N_3O_5S_2$: C, 50.61; H, 3.25; N, 10.42; S, 15.89%; Found: C, 50.54; H, 3.19; N, 10.39; S, 15.92%; GC–MS *m/z*: 403.6 ($M^{\cdot+}$).

4.2.13. 1-(2-Thienylcarbonyl)-3-(4-aminosulfonylphenyl)thiourea (**5b**)

Yield: (78%); m.p 225 °C; IR (Pure) υ: 3245 (NH), 1660 (C═O), 1590 (C═S), 1531 (thioamide I), 1330 (C–S), 1234 (thioamide II), 1151, 1097 (thioamide III), 747 (thioamide IV) cm^{-1}; ^{1}H NMR (δ ppm, *J* Hz): 11.8 (s, 1H, NH), 9.81 (s, 1H, NH), 7.51 (d, 1H, thiophenyl, J = 5.3), 7.97 (d, 2H, Ar, J = 6.1), 7.15 (d, 2H, Ar, J = 6.5),6.73 (d, 1H, thiophenyl, J = 6.51), 6.67 (d, 1H, thiophenyl, J = 6.5), 7.62 (d, 2H, Ar, J = 6.3), 6.51 (d, 2H, Ar, J = 5.9);^{13}C NMR (δ ppm): 180.7 (C═S), 171.4 (C═O), 144.1 (thiophenyl), 139 (C–N), 137.3, 136.4, 133 (Ar), 131 (Ar), 129 (Ar), 128 (Ar). Anal. Calcd. For $C_{12}H_{11}N_3O_3S_3$: C, 42.22; H, 3.25; N, 12.31; S, 28.17; Found: C, 42.19; H, 3.21%; N, 12.36; S, 28.21%; GC–MS *m/z*: 342.4 ($M^{\cdot+}$).

4.3. Crystallographic study of 1-(2-furanyl)-3-(3-aminosulfonylphenyl)thiourea (**3g**)

Colorless crystal, size 0.40 × 0.08 × 0.06 mm^3, monoclinic space group $P2_1/\mathbf{c}$ with Z = 4, a = 12.8063(10), b = 14.3698(11), c = 7.5479(6) Å, β = 103.271(29°), V = 1351.90(18) Å^3; D_c = 1.599 Mg/m^3, μ = 0.414 mm^{-1}, F(000) = 672. The intensity data were recorded using a Bruker SMART CCD area-detector diffractometer with graphite monochromated MoK_α radiation (λ = 0.71073 Å) at T = 130(2) K. 12,615 reflections collected $1.6 > \Theta > 27.9°$; 3218 independent reflections $I > 2\sigma(I)$. Structure solution by direct method [29], full-matrix least squares refinement [29]based on F^2 and 198 parameters. All but H-atoms were refined anisotropical, hydrogen atoms were clearly located from difference Fourier maps, refined at idealized positions riding on the carbon or nitrogen atoms with isotropic displacement parameters Uiso(H) = 1.2U_{eq}(C/N) and C–H 0.95 Å, N–H 0.88 Å; H(N3) positions were refined freely. Refinement converged at R1 = 0.039 [$I > 2\sigma(I)$], wR2 = 0.099 [all data] and S = 1.032; min./max. ΔF −0.37/0.45 e/Å^3.

Crystallographic data (excluding structure factors) for the structure reported in this paper have been deposited with the Cambridge Crystallographic Data Centre as supplementary publication no. CCDC-954814. Copies of available material can be obtained free of charge via www.ccdc.cam.ac.uk/data_request/cif, by e-mailing data_request@ccdc.cam.ac.uk, or contacting the Cambridge Crystallographic Data Centre, 12, Union Road, Cambridge CB2 1EZ, UK; fax: +44 1223 336033.

4.4. In vitro carbonic anhydrase inhibition

Carbonic anhydrase inhibition was measured by the method [30] after standardization of reaction conditions like enzyme conc., substrate conc., buffer pH, duration of reaction etc. The method is based on the principle that *p*-nitrophenyl acetate is hydrolyzed by CA to form *p*-nitrophenol which was determined spectrophotometrically. Reaction mixture contained 60 μL of 50 mM Tris–sulfate buffer (pH 7.6 containing 0.1 mM $ZnCl_2$), 10 μL (0.5 mM) test compound in 1% DMSO and 10 μL (50 U) bovine enzyme per well. Contents were mixed and preincubated at 25 °C for 10 min. Plates were pre-read at 348 nm using a 96 well plate reader. Substrate, *p*-nitrophenyl acetate was prepared (6 mM stock using <5% acetonitrile in buffer and used fresh) and 20 μL was added per well to achieve 0.6 mM concentration per well. Total reaction volume was made to 100 μL. After30 min incubation at 25 °C, contents were mixed and read at 348 nm. Suitable controls with DMSO and known inhibitor acetazolamide were included in the assay. Results reported are mean of three independent experiments (±SEM) and expressed as percent inhibitions calculated by the formula, Inhibition (%) = [100−(Abs of test comp/Abs of control) × 100]. IC_{50} values of selected compounds exhibiting >50% activity at 0.5 mM were calculated after suitable dilutions.

4.5. Molecular modeling studies of carbonic anhydrase

4.5.1. Structure selection and preparation

Molecular modeling and docking studies were carried out on bovine CA-II (bCA II) and human CA-II (hCA II) enzymes. In order to carry out efficient and accurate modeling studies, high-resolution

3D structures of both enzymes were selected from the Protein DataBank [31]. A high-resolution crystal structure of 1.95 Å (PDB Code: 1V9E) was selected for bCA II and a high-resolution crystal structure of 1.03 Å (PDB Code: 3V7X) was selected for hCA II. The hCA II x-ray structure contains a co-crystalized ligand N-[2-(3,4-dimethoxyphenyl)ethyl]-4-sulfamoylbenzamide (PDB Code: D7A) in its active site. As the structure of bCA II enzyme does not include a co-crystallized ligand, the co-crystalized ligand of hCA II is used for binding site definition and interaction studies.

The enzyme structure was protonated with Protonate3D [32] algorithm implemented in MOE [33]. Protonate3D correctly identified and assigned the protonation states for important residues in the active site and the ligand atoms. Correct charges for the zinc metal (Zn^{2+}), the correct protonation states were assigned for the surrounding histidine residues (His94, His96 and His119) and the nitrogen atom in the sulfamoylbenzamide moiety of D7A ligand. After adding hydrogen atoms and determination of protonation states, the enzyme structures were energy minimized. Gradient-based energy minimization with Amber99 force field was performed with all the heteroatoms and solvent molecules present in the 3D structures and the minimization was allowed to terminate if the root mean square gradient falls below 0.1. The backbone atoms were restrained with a small force constant of 100 in order to avoid collapse of the binding pockets during energy minimization calculations.

4.5.2. Compounds preparation

The 3D structural coordinates of the compounds were generated for all the compounds using MOE followed by assignment of protonation and ionization states in physiological pH range by using the "wash" module. Then compounds' structures were energy minimized with the MMFF94x force field for the docking studies and structures were prepared by using utility programs present in AmberTools [34] to derive AM1-BCC charges and force-field related parameters for the individual compounds.

4.5.3. Docking studies

The binding sites of both enzymes were defined by including residues surrounding around 7.5Å radius of the co-crystallized bound ligands for docking studies. The same co-crystallized ligand (D7A) was used in both enzyme structures for determining the active site. Docking was performed by LeadIT [35] program that utilizes FlexX for the docking calculations. The default docking and scoring parameters were chosen for the docking calculations and the top 10 docked conformations were retained for analyzing the interactions and binding modes.

4.5.4. Pose ranking

The predicted docked poses of each compound were evaluated for interactions with the enzyme to select the most favorable binding mode of a compound. The evaluation was performed by using re-scoring of the docked poses by an external scoring function, NNScore. Sets of top ranking poses were retained for all compounds against both enzymes, which were further evaluated for stability and binding energy estimation with molecular dynamics simulations.

4.5.5. Molecular dynamics simulations

Molecular dynamics (MD) simulations were performed on the ligand-docked structures of bCA II and hCA II complexes. The force field charges for the protein structures were calculated by using Amber [36] force field ff99SB. The force field charges and parameters for the zinc metal complex were derived from ZAFF (Zinc Amber Force Field) [http://pubs.acs.org/doi/abs/10.1021/ct1002626]. AM1-BCC charges were used for the ligands calculated by the Antechamber module of Amber and the parameters for the ligands were adapted from the general amber force field (GAFF) library. The docked enzyme–ligand complexes were solvated using the LeaP module of Amber by using an octahedron box of the TIP3P water model with a distance of 8 Å between the edge of the box and the protein. Using counter sodium ions to neutralize the negatively charged enzyme–ligand complexes neutralized the solvated complexes but most of the enzyme–ligand complexes were already in neutral charge form. This is because the +1 charge of the enzyme was neutralized by the addition of negatively charge ligand molecule. Each individual enzyme–ligand solvated complex system was minimized with 2500 steps of conjugate gradient minimization followed by 2500 steps of steepest decent minimization.

The equilibration steps included 50 ps of heating (from 0 to 300 K temperature), 50 ps of density equilibration with weak restraints on the complex atoms followed by 3 ns of constant pressure equilibration at 300 K. The equilibration process was carried out using Sander program of Amber12 package. Molecular dynamics simulations were performed by using Particle Mesh Ewald (PME) MD program of Amber12 package on the equilibrated complexes. With a step size of 2 fs, the simulations were per-formed for 2 ns time scale and atomic coordinates after each 500 step were saved. The SHAKE algorithm was applied to constrain bonds involving hydrogen atoms with 8 Å van der Waals cut off using the PME method.

4.5.6. Free energy of binding

The binding free energies were estimated by using Molecular Mechanics/Poisson–Boltzmann Surface Area (MM/PBSA) and Molecular Mechanics/Generalized Born Surface Area (MM/GBSA) calculations. MM/PBSA and MM/GBSA based energies were calculated for the snapshots extracted from the 2 ns trajectories that included 2000 snapshots recorded at 1 ps time interval. The interaction energies and salvation free energies were computed for the complex, enzyme and ligand at each 5th frame (snapshot) in the trajectory to obtain statistically meaningful results. Experimental IC_{50} values were transformed to ΔG by the formula: $\Delta G = -RT \ln K_i$

Where R is gas constant, T is temperature in Kelvin (300 K) and K_i (in nM) is the experimental affinity value. A comparison of estimated binding energy values with that of experimentally determined ΔG values for the compounds was carried out to observe correlation between the predicted and experimentally determined binding energy values.

Acknowledgment

This work was financially supported by COMSTECH–TWAS and German-Pakistani Research Collaboration Programme.

Appendix A. Supplementary data

Supplementary data related to this article can be found at http://dx.doi.org/10.1016/j.ejmech.2014.03.023.

References

[1] C.T. Supuran, Carbonic anhydrases: novel therapeutic applications for inhibitors and activators, Nature Reviews Drug Discovery 7 (2008) 168–181.
[2] C. Temperini, A. Innocenti, A. Scozzafava, S. Parkkila, C.T. Supuran, The coumarin-binding site in carbonic anhydrase accommodates structurally diverse inhibitors: the antiepileptic lacosamide as an example and lead molecule for novel classes of carbonic anhydrase inhibitors, Journal of Medicinal Chemistry 53 (2009) 850–854.
[3] F. Mincione, A. Scozzafava, C.T. Supuran, Antiglaucoma Carbonic Anhydrase Inhibitors as Ophthalomologic Drugs, Wiley, Hoboken (NJ), 2009.

[4] A. Thiry, J.M. Dogne, B. Masereel, C.T. Supuran, Targeting tumor-associated carbonic anhydrase IX in cancer therapy, Trends in Pharmacological Sciences 27 (2006) 566–573.
[5] P. Ebbesen, E.O. Pettersen, T.A. Gorr, G. Jobst, K. Williams, J. Kieninger, R.H. Wenger, S. Pastorekova, L. Dubois, P. Lambin, B.G. Wouters, T. Van Den Beucken, C.T. Supuran, L. Poellinger, P. Ratcliffe, A. Kanopka, A. Gorlach, M. Gasmann, A.L. Harris, P. Maxwell, A. Scozzafava, Taking advantage of tumor cell adaptations to hypoxia for developing new tumor markers and treatment strategies, Journal of Enzyme Inhibition and Medicinal Chemistry 24 (Suppl. 1) (2009) 1–39.
[6] M. Hilvo, A.M. Salzano, A. Innocenti, M.S. Kulomaa, A. Scozzafava, A. Scaloni, S. Parkkila, C.T. Supuran, Cloning, expression, post-translational modifications and inhibition studies on the latest mammalian carbonic anhydrase isoform, CA XV, Journal of Medicinal Chemistry 52 (2009) 646–654.
[7] V. Alterio, R.M. Vitale, S.M. Monti, C. Pedone, A. Scozzafava, A. Cecchi, G. De Simone, C.T. Supuran, Carbonic anhydrase inhibitors: X-ray and molecular modeling study for the interaction of a fluorescent antitumor sulfonamide with isozyme II and IX, Journal of the American Chemical Society 128 (2006) 8329–8335.
[8] A.A. Sh Ali, S.A. Al-Mashta, Cerebral calcification, osteopetrosis and renal tubular acidosis: is it carbonic anhydrase-II deficiency? Saudi Journal of Kidney Diseases and Transplantation: An Official Publication of the Saudi Center for Organ Transplantation, Saudi Arabia 24 (2013) 561–565.
[9] B.S. Avvaru, S.A. Busby, M.J. Chalmers, P.R. Griffin, B. Venkatakrishnan, M. Agbandje-McKenna, D.N. Silverman, R. McKenna, Apo-human carbonic anhydrase II revisited: implications of the loss of a metal in protein structure, stability, and solvent network, Biochemistry 48 (2009) 7365–7372.
[10] F.M. Gribble, F. Reimann, Differential selectivity of insulin secretagogues: mechanisms, clinical implications, and drug interactions, Journal of Diabetes and its Complications 17 (2003) 11–15.
[11] J. Drews, Drug discovery: a historical perspective, The New York Academy of Sciences 287 (2000) 1960–1964.
[12] A. Mastrolorenzo, A. Scozzafava, C.T. Supuran, Antifungal activity of silver and zinc complexes of sulfadrug derivatives incorporating arylsulfonylureido moieties, European Federation for Pharmaceutical Sciences: Official Journal of the European Federation for Pharmaceutical Sciences 11 (2000) 99–107.
[13] T.H. Maren, Relatons between structure and biological activity of sulfonamides, Annual Review of Pharmacology and Toxicology 16 (1976) 309–327.
[14] A. Ryckebusch, R. Deprez-Poulain, M.A. Debreu-Fontaine, R. Vandaele, E. Mouray, P. Grellier, C. Sergheraert, Parallel synthesis and anti-malarial activity of a sulfonamide library, Bioorganic & Medicinal Chemistry Letters 12 (2002) 2595–2598.
[15] J. Krungkrai, A. Scozzafava, S. Reungprapavut, S.R. Krungkrai, R. Rattanajak, S. Kamchonwongpaisan, C.T. Supuran, Carbonic anhydrase inhibitors. Inhibition of plasmodium falciparum carbonic anhydrase with aromatic sulfonamides: towards antimalarials with a novel mechanism of action? Bioorganic & Medicinal Chemistry 13 (2005) 483–489.
[16] R. Klingenstein, P. Melnyk, S.R. Leliveld, A. Ryckebusch, C. Korth, Similar structure-activity relationships of quinoline derivatives for antiprion and antimalarial effects, Journal of Medicinal Chemistry 49 (2006) 5300–5308.
[17] K. Ekoue-Kovi, K. Yearick, D.P. Iwaniuk, J.K. Natarajan, J. Alumasa, A.C. de Dios, P.D. Roepe, C. Wolf, Synthesis and antimalarial activity of new 4-amino-7-chloroquinolyl amides, sulfonamides, ureas and thioureas, Bioorganic & Medicinal Chemistry 17 (2009) 270–283.
[18] M.A. Santos, S. Marques, D. Vullo, A. Innocenti, A. Scozzafava, C.T. Supuran, Carbonic anhydrase inhibitors: inhibition of cytosolic/tumor-associated isoforms I, II, and IX with iminodiacetic carboxylates/hydroxamates also incorporating benzenesulfonamide moieties, Bioorganic & Medicinal Chemistry Letters 17 (2007) 1538–1543.
[19] I. Nishimori, T. Minakuchi, T. Kohsaki, S. Onishi, H. Takeuchi, D. Vullo, A. Scozzafava, C.T. Supuran, Carbonic anhydrase inhibitors: the beta-carbonic anhydrase from Helicobacter pylori is a new target for sulfonamide and sulfamate inhibitors, Bioorganic & Medicinal Chemistry Letters 17 (2007) 3585–3594.
[20] M.A. Ilies, C.T. Supuran, A. Scozzafava, Carbonic anhydrase inhibitors. Part 91. Metal complexes of heterocyclic sulfonamides as potential pharmacological agents in the treatment of gastric acid secretion imbalances, Metal-Based Drugs 7 (2000) 57–62.
[21] M. Zareef, R. Iqbal, N.G. De Dominguez, J. Rodrigues, J.H. Zaidi, M. Arfan, C.T. Supuran, Synthesis and antimalarial activity of novel chiral and achiral benzenesulfonamides bearing 1, 3, 4-oxadiazole moieties, Journal of Enzyme Inhibition and Medicinal Chemistry 22 (2007) 301–308.
[22] J. Krungkrai, S.R. Krungkrai, C.T. Supuran, Carbonic anhydrase inhibitors: inhibition of plasmodium falciparum carbonic anhydrase with aromatic/heterocyclic sulfonamides-in vitro and in vivo studies, Bioorganic & Medicinal Chemistry Letters 18 (2008) 5466–5471.
[23] J. Botet, L. Mateos, J.L. Revuelta, M.A. Santos, A chemogenomic screening of sulfanilamide-hypersensitive Saccharomyces cerevisiae mutants uncovers ABZ2, the gene encoding a fungal aminodeoxychorismate lyase, Eukaryotic Cell 6 (2007) 2102–2111.
[24] A. Saeed, S. Zaib, A. Pervez, A. Mumtaz, M. Shahid, J. Iqbal, Synthesis, molecular docking studies, and in vitro screening of sulfanilamide-thiourea hybrids as antimicrobial and urease inhibitors, Medicinal Chemistry Research 22 (2013) 3653–3662.
[25] A. Saeed, M.F. Erben, U. Flörke, Effect of fluorine substitution on the crystal structures and vibrational properties of phenylthiourea isomers, Journal of Molecular Structure 982 (2010) 91–99.
[26] H.M. Faidallah, H.A. Albar, M.S. Makki, E. Sharshira, Synthesis of novel cyclic benzenesulfonylurea and thiourea derivatives, Phosphorus, Sulfur, and Silicon and the Related Elements 177 (2002) 685–693.
[27] A. Saeed, A. Mumtaz, U. Florke, Synthesis, characterization and crystal structure of 1-(4-methylbenzoyl)-3-(4 aminosulfonylphenyl) thiourea, European Journal of Chemistry 1 (2010) 73–75.
[28] A. Saeed, A. Mumtaz, H. Ishida, Synthesis, characterization of some new 1-aroyl-3-(4-aminosulfonylphenyl) thioureas and crystal structure of 1-(3, 4, 5-trimethoxybenzoyl)-3-(4-aminosulfonylphenyl) thiourea, Journal of Sulfur Chemistry 32 (2011) 45–54.
[29] G.M. Sheldrick, A short history of SHELX, Acta Crystallogr. Sect A, Foundations of Crystallography 64 (2008) 112–122.
[30] M. al-Rashida, M. Ashraf, B. Hussain, S.A. Nagra, G. Abbas, Discovery of new chromone containing sulfonamides as potent inhibitors of bovine cytosolic carbonic anhydrase, Bioorganic & Medicinal Chemistry 19 (2011) 3367–3371.
[31] D.S. Goodsell, Computational docking of biomolecular complexes with AutoDock, Cold Spring Harbor Protocols 2009 (2009) pdb.prot5200.
[32] P. Labute, Protonate 3D, 2007. http://www.chemcomp.com/journal/proton.htm.
[33] MOE (The Molecular Operating Environment) Version 2010.10, Chemical Computing Group Inc. http://www.chemcomp.com.
[34] D.A. Case, T.E. Cheatham 3rd, T. Darden, H. Gohlke, R. Luo, K.M. Merz Jr., A. Onufriev, C. Simmerling, B. Wang, R.J. Woods, The Amber biomolecular simulation programs, Journal of Computational Chemistry 26 (2005) 1668–1688.
[35] http://www.biosolveit.de/LeadIT/.
[36] D.A. Case, T. Darden, T.E. Cheatham III, C.L. Simmerling, J. Wang, R.E. Duke, R. Luo, M. Crowley, R.C. Walker, W. Zhang, K.M. Merz, B. Wang, S. Hayik, A. Roitberg, G. Seabra, I. Kolossvary, K.F. Wong, F. Paesani, J. Vanicek, X. Wu, S.R. Brozell, T. Steinbrecher, H. Gohlke, L. Yang, C. Tan, J. Mongan, V. Hornak, G. Cui, D.H. Mathews, M.G. Seetin, C. Sagui, V. Babin, P.A. Kollman, AMBER11, University of California, San Francisco, 2010.